Progress Towards Increased Understanding and Control of Internal Transport Barriers on DIII–D

E.J. Doyle,[1] C.M. Greenfield,[2] M.E. Austin,[3] L.R. Baylor,[4] K.H. Burrell,[2] T.A. Casper,[5] J.C. DeBoo,[2] D.R. Ernst,[6] C. Fenzi,[7] P. Gohil,[2] R.J. Groebner,[2] W.W. Heidbrink,[8] G.L. Jackson,[2] T.C. Jernigan,[4] J.E. Kinsey,[9] L.L. Lao,[2] M. Makowski,[5] G.R. McKee,[7] M. Murakami,[4] W.A Peebles,[1] R. Prater,[2] C.L. Rettig,[1] T.L. Rhodes,[1] J.C. Rost,[10] G.M. Staebler,[2] B.W. Stallard,[5] E.J. Strait,[2] E.J. Synakowski,[6] D.M. Thomas,[2] M.R. Wade,[4] R.E. Waltz[2] and L. Zeng[1]

[1]Dept. of Electrical Engineering and IPFR, University of California, Los Angeles, California 90095, USA.
e-mail: doylej@fusion.gat.com
[2]General Atomics, P.O. Box 85608, San Diego, California 92186, USA
[3]University of Texas at Austin, Austin, Texas 78712, USA
[4]Oak Ridge National Laboratory, Oak Ridge, Tennessee 37381, USA
[5]Lawrence Livermore National Laboratory, Livermore, California, 94550, USA
[6]Princeton Plasma Physics Laboratory, Princeton, New Jersey 08543, USA
[7]University of Wisconsin-Madison, Madison, Wisconsin 53706, USA
[8]University of California, Irvine, California 92697, USA
[9]Lehigh University, Bethlehem, Pennsylvania 18015, USA
[10]Massachusetts Institute of Technology, Cambridge, Massachusetts 02139, USA

Abstract. Substantial progress has been made towards both understanding and control of internal transport barriers (ITBs) on DIII-D, resulting in the discovery of a new sustained high performance operating mode termed the Quiescent Double-Barrier (QDB) regime. The QDB regime combines core transport barriers with a quiescent, ELM-free H-mode edge (termed QH-mode), giving rise to separate (double) core and edge transport barriers. The core and edge barriers are mutually compatible and do not merge, resulting in broad core profiles with an edge pedestal. The QH-mode edge is characterized by ELM-free behavior with continuous multiharmonic MHD activity in the pedestal region, and has provided density and impurity control for 3.5 s (>20 τ_E) with divertor pumping. QDB plasmas are long-pulse high-performance candidates, having maintained a $\beta_N H_{89}$ product of 7 for 5 energy confinement times ($T_i \leq 16$ keV, $\beta_N \leq 2.9$, $H_{89} \leq 2.4$, $\tau_E \leq 150$ ms, DD neutron rate $S_n \leq 4x10^{15}$ s^{-1}). The QDB regime has only been obtained in counter-NBI discharges (injection anti-parallel to plasma current) with divertor pumping. Other results include successful expansion of the ITB radius using (separately) both impurity injection and counter-NBI, and the formation of ITBs in the electron thermal channel using both ECH and strong negative central shear (NCS) at high power. These results are interpreted within a theoretical framework in which turbulence suppression is the key to ITB formation and control, and a decrease in core turbulence is observed in all cases of ITB formation.

1. Introduction

The primary goal of the DIII-D Advanced Tokamak (AT) research program is to optimize the reactor potential of the tokamak concept by achieving a high bootstrap current fraction, while simultaneously maintaining the conditions for fusion power density and gain [1]. Implicit in this goal is the development of an ability to control the location and strength of internal transport barriers (ITBs). Control capabilities are required to sustain the ITB and to realize predicted gains in fusion performance and stability limits: increasing the spatial extent of the barrier increases fusion performance and MHD stability limits, and results in a favorable bootstrap alignment with the total current profile, while control of gradients is required to avoid instabilities and disruptions.

Shown in Fig. 1 is a diagrammatic representation of optimal and non-optimal ITB profiles. Optimized ITB profiles lie at a large radius, ρ_{ITB}, and possess moderate gradients (large ITB half width, $\Delta\rho_{ITB}$), while non-optimal ITB profiles are the opposite. [In this paper we take ρ_{ITB} to lie at the foot of the ITB. For the hyperbolic-tangent profile model used in Fig. 1, $\rho_{ITB} = \rho_{SYM} + \Delta\rho_{ITB}$, where ρ_{SYM} is the symmetry radius of the ITB. In modeling work, ρ_{ITB} is often defined as ρ_{SYM}]. A larger ρ_{ITB} increases fusion performance by increasing the

volume of the improved confinement region, which increases both the maximum pressure and the confinement factor H_{89} ($H_{89} = \tau/\tau_{89}$, where τ_{89} is a confinement scaling expression for L-mode plasmas [2]). MHD modeling indicates that the maximum stable normalized beta, $\beta_N = \beta/(I/aB_\varphi)$, increases by 60% or more as both ρ_{SYM} and $\Delta\rho_{ITB}$ are increased [3]. In addition, modeling of future reactor concepts such as ARIES-AT indicates that obtaining a large bootstrap current fraction, f_{BS}, with good alignment requires $\rho_{SYM} \sim 0.7$-0.8, with moderate to large $\Delta\rho_{ITB}$ [4]. From these considerations it can be seen that *all* of the requirements for successful AT operation, high performance (high $\beta_N H_{89}$, a figure of merit for AT machines [1]), and large, well-aligned bootstrap fraction, imply a requirement for both large ρ_{ITB} and $\Delta\rho_{ITB}$. Consequently,a specific component of the overall DIII-D AT research program is dedicated to developing the control tools required to achieve large ρ_{ITB} and $\Delta\rho_{ITB}$. The results reported here begin to put in place validated experimental and theoretical tools targeted for an integrated demonstration of ITB control within a time scale of a few years.

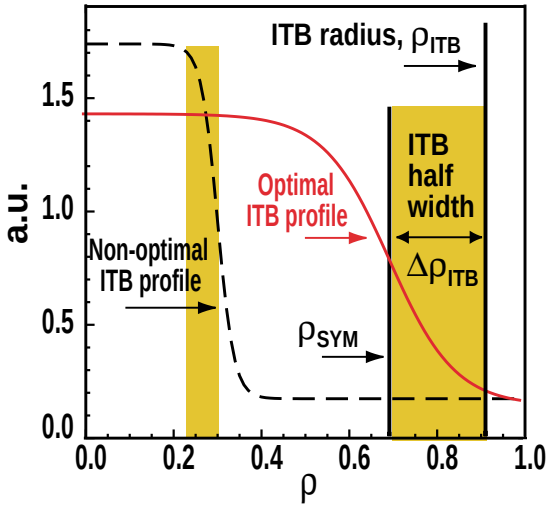

FIG. 1. A diagrammatic representation of optimal (broad profiles with moderate gradients) and non-optimal (narrow profiles with steep gradients) ITB profiles.

2. Transport Barrier Formation – Electron Thermal ITBs

ITBs must first be formed before they can be controlled. An outline summary of our understanding of how ITBs are formed is presented in Table I. In our understanding, turbulence suppression mechanisms are the key to ITB formation and control. However, the various stabilization mechanisms differ with regard to the turbulence wavelengths they affect, such that obtaining transport barriers is not equally possible with all suppression mechanisms [5]. Specifically, the most commonly identified turbulence suppression mechanism on DIII-D, sheared ExB flow [6], affects mainly long wavelength (low-*k*) turbulence. Long wavelength, ITG-type fluctuations are believed to control transport in the ion thermal and angular momentum channels. However, electron thermal transport can be governed by short wavelength, high-*k* ETG-type turbulence, which is not expected to respond to ExB shear, due to smaller spatial scales and larger growth rates [7]. Medium-k turbulence, such as the trapped electron mode (TEM), can generate particle and electron and ion thermal transport, and can be affected by ExB shear, but less so than for the low-*k*, ITG-type turbulence. Thus, it might be expected to be easiest to obtain ITBs in the ion thermal and angular momentum channels, somewhat harder in the particle transport channel, and hardest in the electron thermal channel, which is consistent with observations on DIII-D [8,9] and elsewhere [10]. Other turbulence reduction mechanisms, such as operation with negative central magnetic shear

Table I. An outline summary of our current understanding of how ITBs are formed, indicating a range of turbulence scales, with corresponding turbulence mechanisms, affected transport channels, and stabilization mechanisms.

Indicative turbulence scales	$k_\theta\rho_s$: 0.1 – 1. – 10	k_θ (cm^{-1}): 1. – 10 – 100
Turbulence/ transport mechanisms	ITG	
	TEM	
	ETG	
Affected transport channels	Ion thermal	
	Momentum	
	Electron particle	
	Electron thermal	
Stabilization mechanisms	ExB shear	
	Reversed magnetic shear (NCS)	
	α-stabilization (Shafranov shift)	
	Impurity injection	

(NCS), $\hat{s} = \rho/q\,(dq/d\rho)$, and α–stabilization (Shafranov shift), affect a wider range of turbulence wavenumbers [5,7,11], and allow the formation of electron transport barriers [α is the normalized pressure gradient (ballooning parameter), $\alpha = -q^2 R_o \nabla\beta$, where R_0 is the mean major radius]. Confidence in the above theoretical picture and in theory-based ITB modeling has increased as a consequence of the success of dynamical modeling [12,13] of step-wise ITB expansion previously observed on DIII-D [14].

A series of experiments on DIII-D have demonstrated that electron thermal transport barriers (e-ITBs) can be formed using both strong NCS, $\hat{s} < 0$ [8,9], and with localized direct electron heating using electron cyclotron heating (ECH) [15]. With strong NCS and high power (~8 MW) neutral-beam injection (NBI), simultaneous localized ITBs have been obtained in all four transport channels, with profile gradients and scale lengths similar to those at the plasma edge in H-mode [9]. With ECH, a clear e-ITB with $T_e >> T_i$ forms rapidly after ECH initiation [15]. Analysis using the gyrokinetic linear stability (GKS, [16]) code indicates that in both cases the experimentally measured ∇T_e within the ITB gradient region is very close to the calculated theoretical critical gradient $\nabla T_{e_{crit}}$ for electron temperature gradient (ETG) mode instability, consistent with ETG modes governing electron thermal transport within the barrier region [8,9,15]. Analysis using both the GKS code and a gyro-Landau-fluid transport model (GLF23, [5]) also indicates that α–stabilization is required; without a reduction in turbulence growth rates caused by α–stabilization the calculated $\nabla T_{e_{crit}}$ would be substantially below the experimentally observed ∇T_e [8,15].

The role of α–stabilization in e-ITB formation is illustrated in Fig. 2, which shows the measured T_e profile in a plasma with 0.5 MW of ECH heating, deposited locally at $\rho \sim 0.3$. Also plotted are two simulated T_e profiles from the GLF23 model, which was initialized with fully developed e-ITB profiles and then run to steady-state. The simulation was run with α–stabilization active in one case, inactive in the other. As can be seen, the GLF23 modeling maintains the experimental T_e profile when α–stabilization is allowed, but not without. Similarly, if the GLF23 model is initialized with experimental profiles from before the formation of the e-ITB, the barrier is only observed to form in dynamical simulations if α is sufficiently large [15]. From Table I, it can be seen that α–stabilization should also affect low-*k* turbulence, i.e. conditions for e-ITB formation should also imply a stabilization of low-k turbulence suitable for the formation of an ion thermal ITB (other stabilization mechanisms may also play a role in this). Reflectometer turbulence measurements in the core of ECH-heated plasmas with e-ITB formation indeed show a reduction in low-*k* turbulence at and inside the location of the e-ITB, but not outside. Transport analysis of similar discharges shows that χ_i is at approximately neoclassical levels at and inside the e-ITB, while χ_e is reduced to ~0 in the high gradient ITB region, and increases again inside the ITB [15]. From these results we conclude that α–stabilization and strong NCS can stabilize high-*k* ETG-type turbulence, leading to the formation of electron thermal transport barriers. However,electron thermal transport is still not completely understood. In general, the T_e profile inside e-ITBs is flat, yet the ETG mode is often predicted to be stable in this region, i.e. the turbulence and transport mechanism in the flat profile region is not as yet understood. (The flat central T_e profile in Fig. 2 can be explained by the off-axis ECH deposition.)

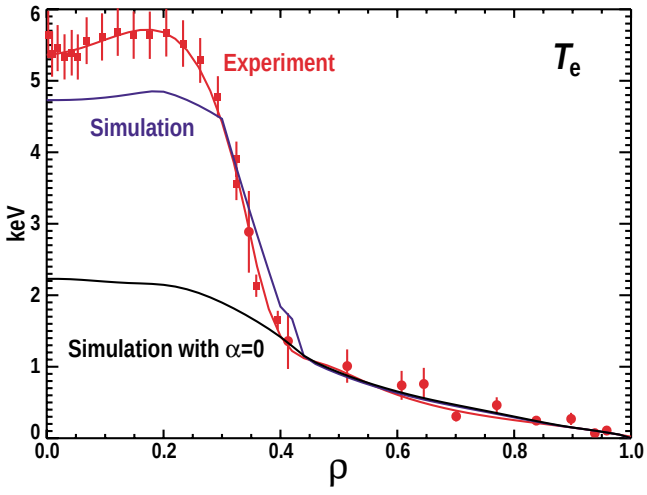

FIG. 2. Example of an experimental electron thermal transport barrier generated by ECH (red curve and data points). Dynamical simulation with the GLF23 transport model maintains the experimental profile if α-stabilization is allowed (blue curve), but not without (black curve).

3. Transport Barrier Expansion

The central challenge of ITB control on DIII-D is to increase ρ_{ITB}. Apart from input power density, the two major factors believed to govern the radius to which ion thermal ITBs expand are the magnetic shear profile and the detailed interplay between rotational and pressure gradient terms in the determination of the ExB shearing rate, ω_{ExB} [17]. Turbulence growth rates are predicted to decrease as $\hat{s}$ is reduced, making it possible for lower levels of E×B shear to suppress turbulence in NCS plasmas as compared to plasmas with positive shear [5,7,11]. This is believed to be one reason why ρ_{ITB} is often observed to lie close to the radius of minimum q, $\rho_{q_{min}}$, in NCS plasmas. Consequently, several attempts have been made to increase ρ_{qmin} as a potential means to increase ρ_{ITB}. A $\rho_{q_{min}}$ of ~0.9 has been obtained using a rapid current ramp and early high power co-NBI, but ρ_{ITB} was still observed to remain at ~0.4–0.5. This result demonstrates that while low or negative $\hat{s}$ may facilitate ITB formation and expansion, it is not a sufficient condition. However, as described below, experiments to increase ρ_{ITB} by impurity injection [18,19], and by varying the interplay between the rotational and pressure gradient terms contributing to ω_{ExB} [17] have proved more successful.

A. Impurity injection

The injection of controlled quantities of impurities has produced significant improvement in plasma performance, on DIII-D [18,19] and elsewhere [20]. A comparison of detailed turbulence data and both linear (GKS) and non-linear (UCAN, [21]) gyrokinetic modeling of impurity (typically neon) injection discharges on DIII-D indicates that the transport improvement on DIII-D is due to the synergism of two effects: Linear growth rates and nonlinear saturated turbulence levels are reduced by the effect of impurity ions on ITG-mode stability, while improved momentum transport results in increased ExB shear, further reducing turbulence levels [18,19]. Previous impurity injection work on DIII-D was performed with L-mode plasmas. In more recent work, impurities have been injected into co-injection discharges with a pre-existing ITB and an L-mode edge, with the intention of expanding ρ_{ITB}. Initial results are encouraging. As shown in Fig. 3, neon injection (2.1 Tℓ/s) results in broader ITB profiles and higher temperatures as compared with an otherwise identical discharge without neon

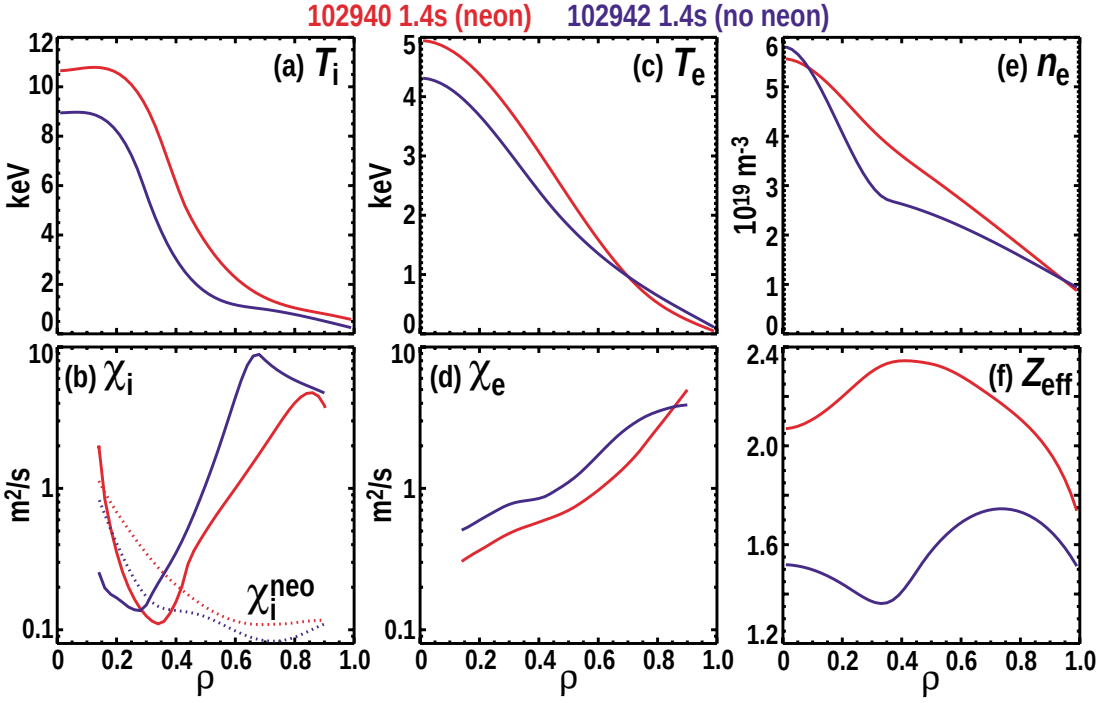

FIG. 3. Profiles of (a) T_i, (b) χ_i and χ_i neoclassical (dashed lines), (c) T_e, (d) χ_e, (e) n_e, and (f) Z_{eff}, for two otherwise identical discharges, one with neon injection (red curves), and a reference case with no neon (blue curves).

injection. As can be seen from the T_i profiles, ρ_{ITB} has been successfully expanded to $\rho \sim 0.7$, while the ion and electron thermal diffusivities indicate that transport is reduced out to $\rho \sim 0.8$. At the time shown in Fig. 3, the neutron rate with neon injection was ~50% higher than in the non-neon case, while the stored energy was increased by ~25%. In agreement with our "standard model" of ITB development, turbulence measurements with both an FIR scattering system and beam emission spectroscopy (BES) indicate a further decrease in the turbulence level, ñ/n, with neon injection.

B. Counter-NBI injection

A detailed consideration of the interplay between rotational and pressure gradient terms, calculated for the main (dueterium) ions, in the expression for the ExB shearing rate, ω_{ExB} [17], has shown that counter-NBI (injection anti-parallel to plasma current) is favorable for ITB expansion. As shown in Fig. 4(a), with co-NBI the rotational and pressure driven components of ω_{ExB} oppose each other, with the rotation term dominating. Consequently, if ∇P is increased (due to an improved ITB), then the ∇P component of the shearing rate will increase, *but this will decrease the total shearing rate, hindering further expansion of the ITB.* As shown in Fig. 4(b), this result is reversed for counter-NBI. With counter-NBI, the rotation and pressure terms still oppose, but now the pressure term dominates and the rotation term is much reduced compared with co-NBI. In this case, if the ∇P component of the shearing rate is increased, *this will increase the total shearing rate, facilitating further expansion of the ITB.* A comparison of ITB profiles in co- and counter-NBI plasmas with similar input powers and L-mode edges shows that ρ_{ITB} is indeed larger in the latter, increasing from $\rho \sim 0.5$ in the co-NBI plasma to $\rho \sim 0.7$ with counter-NBI [17].

4. Quiescent Double Barrier (QDB) Regime

With counter-NBI and divertor pumping, a new quiescent ELM-free H-mode regime was obtained in 1999 with density and impurity control, termed QH-mode [22,23]. This year, the combination of a QH-mode plasma edge and broad counter-injection ITBs resulted in increased plasma performance. This new, high performance operating mode with separate (double) core and edge transport barriers is termed the QDB regime (so-called after the [ELMy] JET double-barrier (DB) mode [24]). To date, the QDB regime has only been obtained in counter-NBI discharges with divertor pumping. The ELM-free QH-mode edge, described in more detail in Refs. [22,23], is characterized by continuous multiharmonic MHD activity in the pedestal region. QH-mode operation has provided density and impurity control

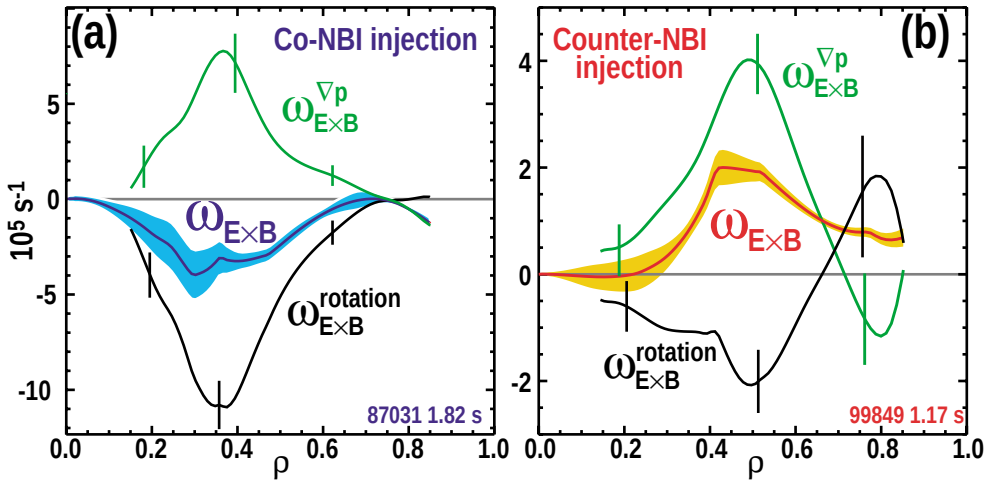

FIG. 4. Main ion pressure gradient (green) and rotation terms (black) of the total ExB shearing rate for (a) co- and (b) counter-NBI discharges. Increasing or broadening the pressure profile will decrease the total ω_{ExB} for co-injection, but increase ω_{ExB} for counter-injection. The total shearing rate is calculated from impurity ion measurements, the pressure gradient term is calculated from the main ion thermal density profile, and the rotation term is obtained by subtraction.

for 3.5 s (>20 τ_E). The distinct core and edge barriers obtained in QDB operation are shown in Fig. 5, which compares QDB profiles with profiles from a counter-NBI ITB plasma with an L-mode edge. With QDB operation the core and edge barriers are mutually compatible and do not merge (ITBs are incompatible with giant ELMs on DIII-D), resulting in broad core profiles with clear edge pedestals in T_i and T_e. Maximum central ion temperatures of 19 keV have been achieved, and the temperature pedestals substantially increase plasma performance relative to the L-mode edge case. In both cases the q profile is reversed (NCS operation), and the foot of the core barrier lies substantially outside $\rho_{q_{min}}$, as shown by the extent of the region of reduced χ_i, which reaches neoclassical levels in the plasma core. The density profile is peaked, favorable for fusion reactivity, while the low edge density is favorable for NBI, ECH/ECCD and pellet access.

As illustrated in Fig. 6, QDB plasmas are long-pulse high-performance candidates, having maintained a $\beta_N H_{89}$ product of 7 for 5 energy confinement times. This was an upper single-null, diverted discharge with the following parameters: I_p = -1.3 MA (reversed plasma current), B_T = 2.0 T, $P_{NBI} \leq 12$ MW, $W \leq 1.5$ MJ, $T_i \leq 16$ keV, $\beta_N \leq 2.9$ %-m-T/MA, $H_{89} \leq 2.4$, $\beta_T \leq 3.3\%$, $\tau_E \leq 150$ ms, DD neutron rate $S_n \leq 4\text{x}10^{15}$ s^{-1}, $f_{BS} \leq 0.45$, $Z_{eff}(0) \sim 2.5$ and $q_{min} > 1$. The quoted H_{89} factor and confinement times are after correction for prompt beam ion orbit losses. The discharge is beam fueled, and the density rise is attributable to the increase in beam power with time; discharges with constant beam input power display almost constant density as a function of time. The ELM-free period lasted 2.6 s, and impurity control during this time is demonstrated by the constant radiated power fraction. The high performance phase of this discharge lasted >5τ_E, and was terminated by the end of high power NBI injection.

Data from an FIR scattering system indicate that broadband turbulence is reduced across most of the plasma diameter throughout the QDB phase of these discharges [25]. Reflectometer measurements of the turbulence radial correlation length Δr, shown in Fig. 7, indicate a

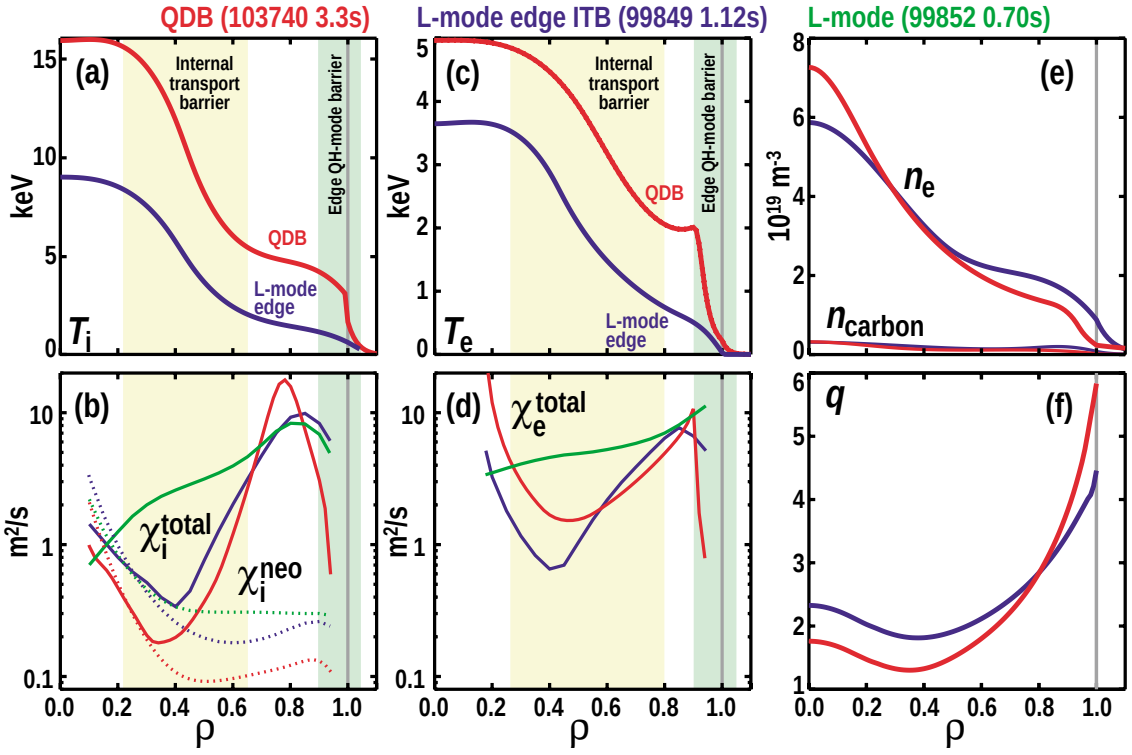

FIG. 5. Profiles of (a) T_i, (b) χ_i total (conduction plus convection) and χ_i neoclassical (dashed lines), (c) T_e, (d) χ_e total, (e) n_e and carbon density, and (f) q, for two discharges. One is a QDB plasma (red curves), the other a counter injection ITB discharge with L-mode edge (blue). The double barrier in the QDB plasma is immediately apparent in the temperature profiles. To better show the region of reduced transport, diffusivities from an L-mode reference discharge are shown (green) in (b) and (d).

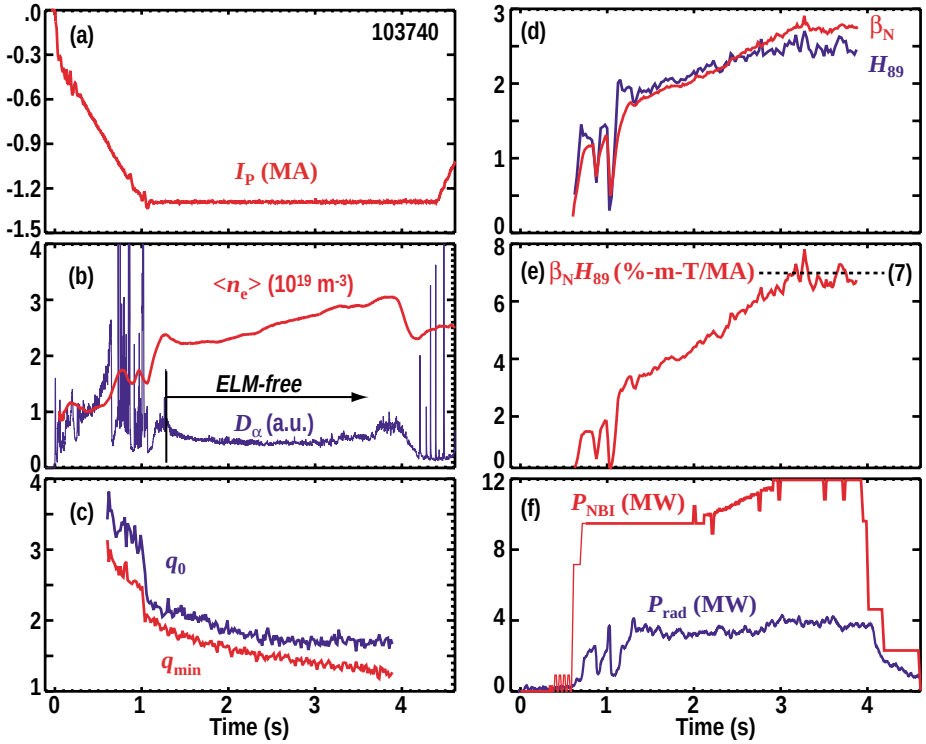

FIG. 6. Time history of the highest performance QDB plasma, showing: (a) I_p, (b) line average density and $D\alpha$, (c) q_0 and q_{min}, (d) β_N and H_{89}, (e) $\beta_N H_{89}$, and (f) P_{NBI} and P_{rad}.

substantial (factor of ~4-8) reduction in Δr over a measurement range of $0.1 \le \rho \le 0.4$ in QDB plasmas, with smaller reductions outside $\rho \sim 0.4$. The reduction is by comparison with previous L-mode measurements [26], in which Δr was found to scale approximately with $\rho_{\theta,s}$ (or 5-8ρ_s). A reduction in the turbulence correlation length should be indicative of a reduction in the step size of the turbulent transport.

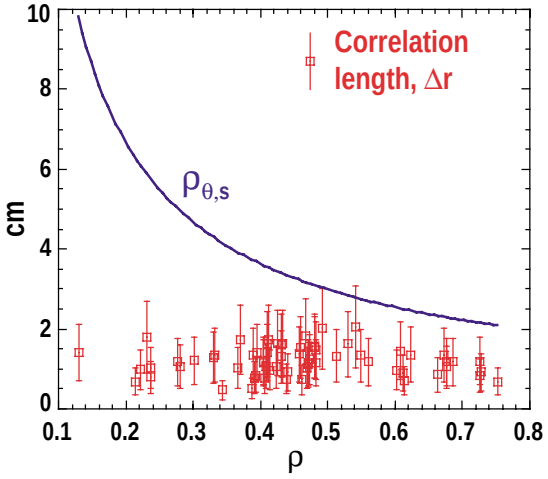

FIG. 7. Reflectometer measurements of the turbulence radial correlation length, Δr, in QDB plasmas, showing a substantial reduction as compared to an approximate scaling with $\rho_{\theta,s}$ observed in L-mode plasmas.

Finally, these QDB plasmas possess several features favorable for next-step devices. Foremost of these is the elimination of the large transient divertor heat loads associated with ELMing H-mode operation, which place a severe constraint on divertor designs. Second, QDB plasmas have exhibited a level of performance substantially in excess of "standard" H-mode levels ($\beta_N H_{89} \le$ 4-5), and are believed to have substantial potential for higher performance. Third, the long-pulse capability of the QDB regime, combined with high edge temperatures and a centrally peaked density profile, may make this an attractive target for ECCD current drive, as well as for other ITB control tools such as off-axis ECH, pellet injection and NBI modulation. Future modeling activity will explore how the counter-NBI used in these experiments could be replaced. For example, ways to create a QH-mode edge might include a dedicated edge beam, edge resonant rf heating, or an ergodic edge layer.

5. Summary and Future Directions

Substantial progress has been made towards both understanding and control of internal transport barriers (ITBs) on DIII-D. DIII-D results are interpreted within a theoretical framework in which turbulence suppression is the key to ITB formation and expansion, and a reduction in core turbulence is observed in all cases of ITB formation. ITB control tools such as counter-NBI, impurity injection and ECH/ECCD are under development, and the spatial extent of the ITBs on DIII-D has been expanded to $\rho \sim 0.6$-0.7. ITBs in the electron thermal channel have been formed using both ECH and strong negative central shear at high power. Most importantly, a new sustained high performance operating mode has been obtained, termed the QDB regime. The QDB regime combines core transport barriers with a quiescent, ELM-free H-mode edge (QH-mode), giving rise to separate (double) core and edge transport barriers. QDB plasmas are long-pulse high-performance candidates, having maintained a $\beta_N H_{89}$ product of 7 for 5 energy confinement times. Future work will explore the scaling and robustness of the QDB regime, which to-date has only been investigated over a limited operating space, and potential further performance increases will be pursued. Modeling work will be initiated to explore the fully non-inductive, steady-state potential of this regime. Finally, the sustained, quasi-steady state nature of the QDB plasmas makes them an attractive target for further ITB control tool development.

Acknowledgments

Work supported by U.S. Department of Energy under Grant Nos, DE-FG03-86ER53225,DE-FG03-97ER54415,DE-FG02-92ER54139, DE-FG02-94ER54235 and Contract Nos. DE-AC03-99ER54463, W-7405-ENG-48, DE-AC05-96OR22725, DE-AC02-76CH03073.

References

[1] PETTY, C.C., et al., "Advanced Tokamak Physics in DIII-D," accepted for publication in Plasma Phys. Control. Fusion (2000).
[2] YUSHMANOV, P.N., et al., Nucl. Fusion **30**, 1999 (1990) .
[3] LAO, L.L., et al., Bull. Am. Phys. Soc. **44**, 77 (1999) .
[4] CHAN, V.S., et al., Bull. Am. Phys. Soc. **44**, 79 (1999).
[5] WALTZ, R.E., et al., Phys. Plasmas **4**, 2482 (1997).
[6] BURRELL, K.H., Phys. Plasmas **4**, 1499 (1997).
[7] JENKO, F., et al., Phys. Plasmas **7**, 1904 (2000) .
[8] STALLARD, B.W., et al., Phys. Plasmas **6**, 1978 (1999) .
[9] DOYLE, E..J. et al., Plasma Phys. Control. Fusion **42**, A236 (2000).
[10] SHIRAI, H. et al., Nucl. Fusion **39**, 1713 (1999).
[11] BEER, M.A., et al., Phys. Plasmas **4**, 1792 (1997).
[12] KINSEY, J.E. et al., "Dynamic Modeling of Step-wise Internal Transport Barrier Formation in DIII-D NCS Discharges," submitted to Phys. Rev. Lett. (2000).
[13] STAEBLER, G.M., et al., paper TH4/1, these proceedings.
[14] GREENFIELD, C.M., et al., Nucl. Fusion **39**, 1723 (1999) .
[15] GREENFIELD, C.M., et al., Proc. of the 27th EPS Conf. on Controlled Fusion and Plasma Physics, Budapest, Hungary, 2000 (European Physical Society, 2000).
[16] WALTZ, R.E., et al., Phys. Plasmas **6**, 4265 (1999).
[17] GREENFIELD, C.M., et al., Phys. Plasmas **7**, 1959 (2000).
[18] McKEE, G.R. , et al., Phys. Plasmas **7**, 1870 (2000) .
[19] MURAKAMI, M., et al., paper EX5/1, these proceedings.
[20] A.M. MESSIAEN, *et al.*, Phys. Rev. Lett. **77** (1996) 2487.
[21] SYDORA, R.D. , et al., Plasma Phys. Control. Fusion **38**, A281 (1996) .
[22] GROEBNER, R.J. et al., paper EXP5/21, these proceedings.
[23] BURRELL, K.H., et al., "Quiescent Double-Barrier H-mode Plasmas in the DIII-D Tokamak," to be submitted to Phys. Plasmas (2000).
[24] SÖLDNER, F.X., et al., Nucl. Fusion **39**, 407 (1999).
[25] ALLEN, S.L, and the DIII-D Team, paper OV1/3, these proceedings.
[26] RHODES, T.L., et al., Proc. of the 27th EPS Conf. on Controlled Fusion and Plasma Physics, Budapest, Hungary 2000 (European Physical Society, 2000).